

Runout analysis of landslides using material point method

Y SUN, J YANG and E SONG

Department of Civil Engineering, Tsinghua University, Beijing 100084, China

E-mail: sunyj12@mails.tsinghua.edu.cn

Abstract. Dynamic simulation of runout landslides is essential for assessment, prevention and mitigation of landslide-induced disasters, but difficult for traditional numerical methods. This paper use the material point method (MPM) to simulate the long runout landslides. The basic theories and the solution procedure of MPM are presented first. Then a landside experiment with the soil modelled by aluminium bars is simulated to validate this method for landslide analysis. The numerical results of the final configuration and the failure surface of the landslide agree well with the experiment results. Finally, the landslide of Erman Mountain in China Sichuan province is simulated. The velocities, affected areas, flow intensity and impact forces on structures are investigated.

1. Introduction

The simulation of long runout landslides such as debris flows, avalanches and large-scale liquefaction failures is very important for determining affected areas and flow intensity, which are essential for assessment, prevention and mitigation of these disasters[1]. Traditional numerical methods such as finite element method, finite volume method, finite difference method and boundary element method are hard to deal with problems in these fields due to mesh tangling, free surface tracking, dissipation problem associated with convection and inherent problems such as modelling slipping, contact and separation. Some meshfree methods such as smoothed particle hydrodynamics and discrete element method suffer from lower accuracy and higher computational cost. The material point method (MPM), developed recently, has enormous advantages in managing problems involving very large deformation and dynamic process[2,3].

MPM developed by Sulsky et al.[4,5] is an extension of the particle-in-cell method [6] to solid mechanics problems. A solid is discretized by a collection of particles (or material points), which carry all the material information. The particles are followed throughout the deformation of the solid and provide a Lagrangian description. A background grid, which can be held fixed or adapted as needed, is used to determine spatial gradients, formulate and solve the governing equations of updated Lagrangian form. The MPM combines the advantages of both Eulerian and Lagrangian schemes, the problem of mesh distortion, which leads to numerical difficulties in the Lagrangian frame, is avoided. The MPM is most suitable for the simulation of large deformation problems.

This paper presents the simulation of long runout landslides by the MPM. The simulation procedure is as follows: (1) The initial stress field within the stable slope is generated with K_0 procedure or gravity loading. (2) A landslide is triggered by decreasing the strength of the soil[7]. (3) The dynamic evolution of the long runout landslides is simulated. At first, a simple numerical example of a 2D landslide experiment conducted by Bui et al.[8] is presented to investigate the accuracy of the MPM in runout analysis. The numerical results of the final configuration and the failure surface of the landslide agree well with the experiment results. Then, the landslide of Erman Mountain in China Sichuan



province, which caused 20 casualties and the destruction of many buildings with about one million cubic meters of debris on July 27, 2010, is simulated by the MPM. The velocities, affected areas, flow intensity and impact forces on the structures are investigated.

2. Material point method

The material point method can be regarded as a special updated Lagrangian finite element method with material point discretization of material and finite element discretization of space. Within the MPM, large deformation is handled by particles moving through a computational grid, which is fixed in space. The followings are the basic theories of MPM[9].

2.1. Governing equations

The governing equations on the current configuration can be formulated in updated Lagrangian form as follows,

$$\sigma_{ij,j} + \rho b_i = \rho \ddot{u}_i, \quad \text{in } \Omega \quad (1)$$

with the boundary conditions

$$\begin{cases} n_j \sigma_{ij} = \bar{T}_i, & \text{on } S_\sigma \\ u_i = \bar{u}_i, & \text{on } S_u \end{cases} \quad (2)$$

where $ij=1,2,3$ are spatial coordinate indices and obey Einstein summation convention; σ_{ij} is the Cauchy stress tensor; ρ is the current material density; b_i is the body force per unit mass; u_i is the displacement, a superposed dot denotes material differentiation with time; Ω , S_σ and S_u are the material domain, the traction boundary and the displacement boundary, respectively; n_j is the unit outward normal vector of S_σ ; \bar{T}_i is the surface traction; \bar{u}_i is the displacement of S_u .

The weak form of the governing equations is

$$\int_{\Omega} \delta u_{i,j} \rho \sigma_{ij}^s dV + \int_{\Omega} \delta u_i \rho \ddot{u}_i dV - \int_{\Omega} \delta u_i \rho b_i dV - \int_{S_\sigma} \delta u_i \rho \bar{T}_i dA = 0 \quad (3)$$

where $\sigma_{ij}^s = \sigma_{ij}/\rho$ and $\bar{T}_i^s = \bar{T}_i/\rho$.

2.2. Material point discretization of material

In MPM, solid bodies are discretized into particles (see Figure 1), termed material points, which carry all the state information such as masses, velocities and stresses.

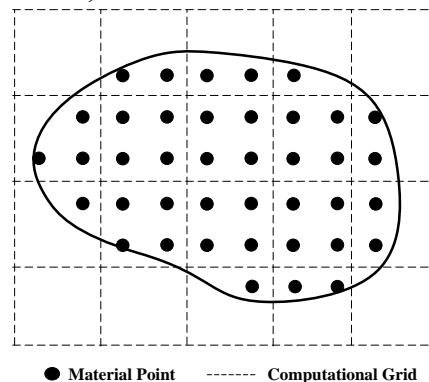


Figure 1. Material point discretization.

The density of an arbitrary point of the soil body is approximated by

$$\rho(x_i) = \sum_{p=1}^{n_p} m_p \delta(x_i - x_{ip}) \quad (4)$$

where the subscript p denotes the material point number, x_i ($i=1,2,3$) is the coordinate of the point, n_p is the number of material points, m_p is the mass of material point p , $\delta(x)$ is Dirac Delta function, x_{ip} is the coordinate of material point p .

2.3. Finite Element Discretization of space

The computational space is subdivided into finite elements $e=1$ to n_e with n_I nodes. Inside each computational step, the computational grid is binded to the material points and deform with the material points. Any variables on the material point can be interpolated from the computational grid nodes by interpolation functions $N_I=N_I(\mathbf{x})$. Linear B-spline interpolation function is adopted in standard MPM.

The finite element trial function u_i is

$$u_i = N_I u_{iI} \quad (5)$$

The test function δu_i is

$$\delta u_i = N_I \delta u_{iI} \quad (6)$$

where the subscript I denotes the computational grid node number. u_{iI} and δu_{iI} are the nodal value of the trial function and test function, respectively. δu_{iI} is zero on displacement boundary S_u and arbitrary otherwise.

2.4. Global equations

Substituting Equation (4),(5) and (6) into Equation (3) leads to

$$m_{IJ} \ddot{u}_{iJ} = f_{iI}^{\text{ext}} - f_{iI}^{\text{int}}, \quad x_I \notin S_u \quad (7)$$

where mass

$$m_{IJ} = \sum_{p=1}^{n_p} m_p N_{Ip} N_{Jp} \quad (8)$$

In MPM, the lumped mass matrix

$$m_{II} = \sum_{J=1}^{n_I} \sum_{p=1}^{n_p} m_p N_{Ip} N_{Jp} = \sum_{p=1}^{n_p} m_p N_{Ip} \quad (9)$$

is usually adopted to reduce the cost of calculation, and the Equation (7) becomes

$$m_{II} \ddot{u}_{iI} = f_{iI}^{\text{ext}} - f_{iI}^{\text{int}}, \quad x_I \notin S_u \quad (10)$$

The external force

$$f_{iI}^{\text{ext}} = \sum_{p=1}^{n_p} N_{Ip} m_p b_{ip} + \sum_{p=1}^{n_p} N_{Ip} \frac{m_p}{\rho_p} \bar{T}_{ip} h^{-1} \quad (11)$$

where h is the thickness of the traction boundary surface, and the internal force

$$f_{iI}^{\text{int}} = \sum_{p=1}^{n_p} N_{Ip,j} \frac{m_p}{\rho_p} \sigma_{ijp} \quad (12)$$

Adopting an explicit scheme over time increment Δt , we get the updated velocities of the background grid nodes from Equation (10).

$$\dot{u}_{il}^{k+1} = \frac{f_{il}^{\text{ext}} - f_{il}^{\text{int}}}{m_{il}} \Delta t + \dot{u}_{il}^k \quad (13)$$

with the subscript k being a time step counter.

The maximum time step is estimated using the CFL stability condition[10]

$$\Delta t_{\text{cr}} \approx \min\left(\frac{\Delta x}{c_p}\right) \quad (14)$$

where Δx is the cell length, c_p is the longitudinal wave speed. The time step size $\Delta t = \alpha_c \Delta t_{\text{cr}}$, $\alpha_c (\leq 1)$ is the time step scale factor called Courant number.

2.5. Solution procedure

Each calculation step of MPM can be classified in three phases[11]: Initial phase where the information of the material points is mapped to the computational grid node to provide initial values for the solution of global equations; Lagrangian phase where the global equations are setup within updated Lagrangian framework and solved to get the nodal velocities and displacements, then the state information, such as locations, velocities and stresses, of the material points are updated; and the convective phase where the computational grid is reset, while keeping the location of the material points constant.

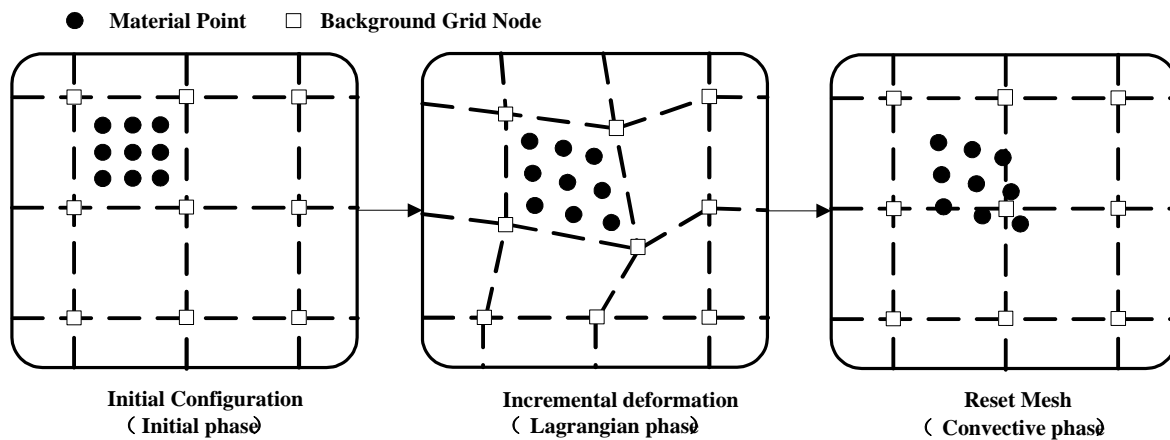


Figure 2. Three phases of one computational step with MPM.

The numeric procedure of one MPM step is as follows.

- (1) Map the momenta, external forces and internal forces of material points to the regular background grid nodes
- (2) Impose the essential boundary conditions on the background grid nodes.
- (3) Solve Equation (13) to update the nodal velocities.
- (4) Update the velocities and positions of the material points using interpolation of the nodal accelerations and updated nodal velocities, respectively.
- (5) Remap the velocities of the material points to the background grid nodes to calculate the incremental strain tensor and the incremental vorticity tensor of the material points. Then update the stress tensor by an objective constitutive model, as well as the density of the material points. In this paper, we adopt an incremental elastoplastic constitutive model

$$\sigma_{ij}^{\nabla} = C_{ijkl}^{ep} \dot{\epsilon}_{kl} \quad (15)$$

with Jaumann stress rate:

$$\dot{\sigma}_{ij}^{\nabla} = \dot{\sigma}_{ij} - W_{jk}\sigma_{ki} - W_{ik}\sigma_{kj} \quad (16)$$

where, W_{ij} is vorticity tensor

$$W_{ij} = \frac{1}{2} \left(\frac{\partial v_i}{\partial x_j} - \frac{\partial v_j}{\partial x_i} \right) \quad (17)$$

and the strain tensor

$$\dot{\epsilon}_{kl} = \frac{1}{2} \left(\frac{\partial v_i}{\partial x_j} + \frac{\partial v_j}{\partial x_i} \right) \quad (18)$$

(6) Reset the deformed grid and use the initial regular background grid in the next step.

3. Numerical examples

Two examples are presented to demonstrate the capabilities of the MPM in capturing the behaviour of long runout landslide, that is: a landslide experiment simulation; Erman Mountain landslide simulation.

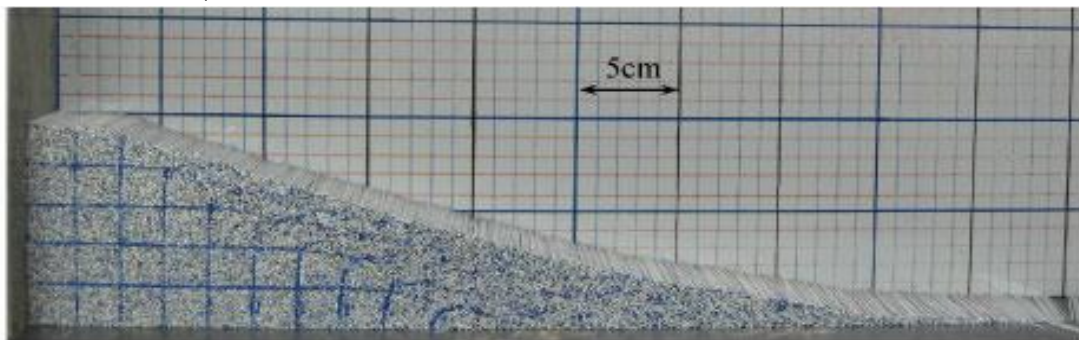
3.1. Landslide experiment simulation

A plane strain experiment of soil collapse was conducted by Bui et al.[8] using small aluminum bars to model the soil. To determine the parameters for the Mohr Coulomb constitutive model of the aluminum bars, they conducted a shear box test. The material parameters are shown in Table 1. This soil model was initially arranged into a rectangular area (200mm×100mm), which is generated by standing two flat solid walls on a flat surface. The simulated slide was triggered by quickly removing the right wall horizontally to the right.

Table 1. Material constants of the aluminum bars

Density(ρ)	Young's modulus(E)	Poisson's ratio(ν)	Cohesion(c)	Friction angle(ϕ)	Dilatancy angle(ψ)
2650 kg/m ³	0.84 MPa	0.3	0 kPa	19.8°	0°

The numerical model is constructed in plane strain condition with symmetric boundary condition and frictional boundary condition at the left and bottom side, respectively. The friction angle δ between the aluminum bars and the flat surface at the bottom equal to the friction angle of aluminum bars, that is $\delta = \phi$. The calculation is performed using square elements with the side length of $\Delta x = 2$ mm and a time step size of $\Delta t = 48.41 \mu s$. Initially, There are 4 material points per element. The initial stress field is generated by K_0 procedure with $K_0 = 1 - \sin(\phi)$.



a.

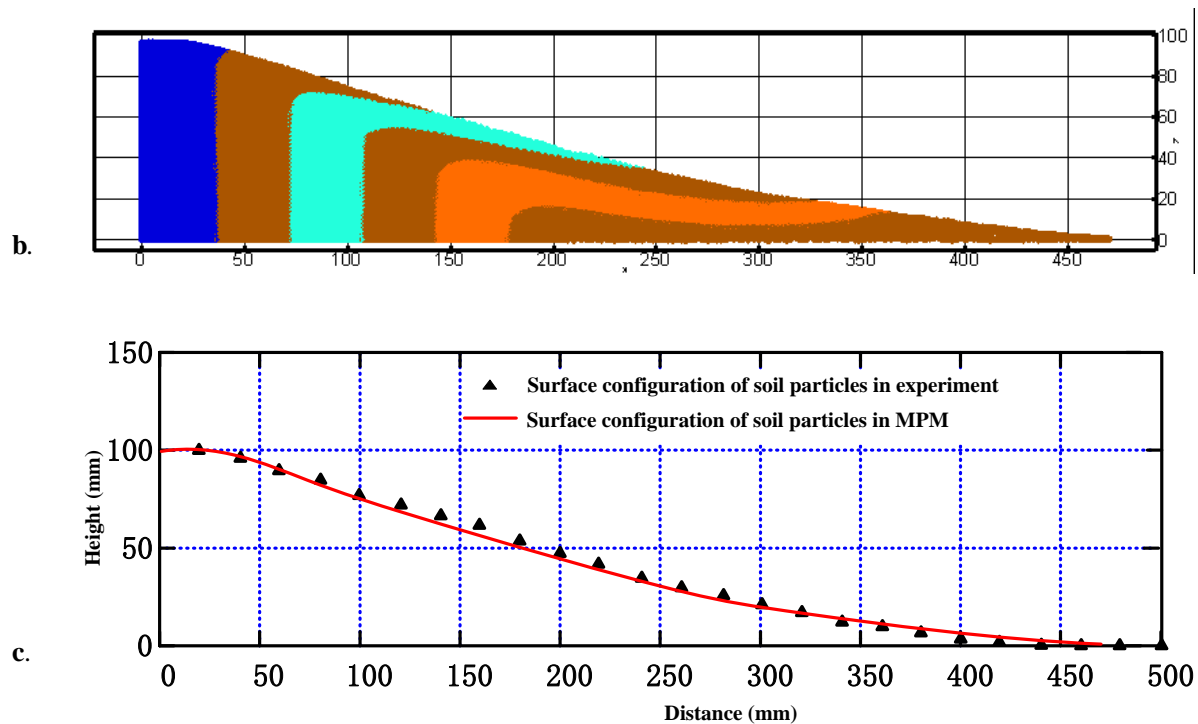


Figure 3. Comparison between experiment and MPM simulation of soil failure.

(a) Experimental result; (b) MPM simulation result; (c) Comparison of surface configurations.

Figure 3 shows the results of the experiment and the computation. Figure 3a is the failure configuration of the experimental result. Figure 3b shows the failure configuration of the MPM simulation result. Figure 3c is the comparison of the free surfaces of the final configuration by the experimental and MPM simulation. From the comparison, we can find that the results of the MPM simulation agree well with those of the experiment. So MPM has the capacity to simulate problems involving very large deformation.

3.2. Erman Mountain landslide simulation

The Erman Mountain lies in China Sichuan province and the landslide took place on July 27, 2010 affecting approximately $48 \times 10^4 \text{ m}^3$ of weathered basalt. The landslide was caused by long time rainfall and consisted of two sliding phases. The first sliding caused 20 casualties and destroyed 5 buildings. After 30mins of the first sliding, the secondary landslide started and ran into the Wangong town at foot of the mountain. The secondary landslide damaged 92 buildings and the evacuation 1500 people[12]. The images of the landslide are shown in Figure 4 and the geological longitudinal section (A-A') is shown in Figure 5.

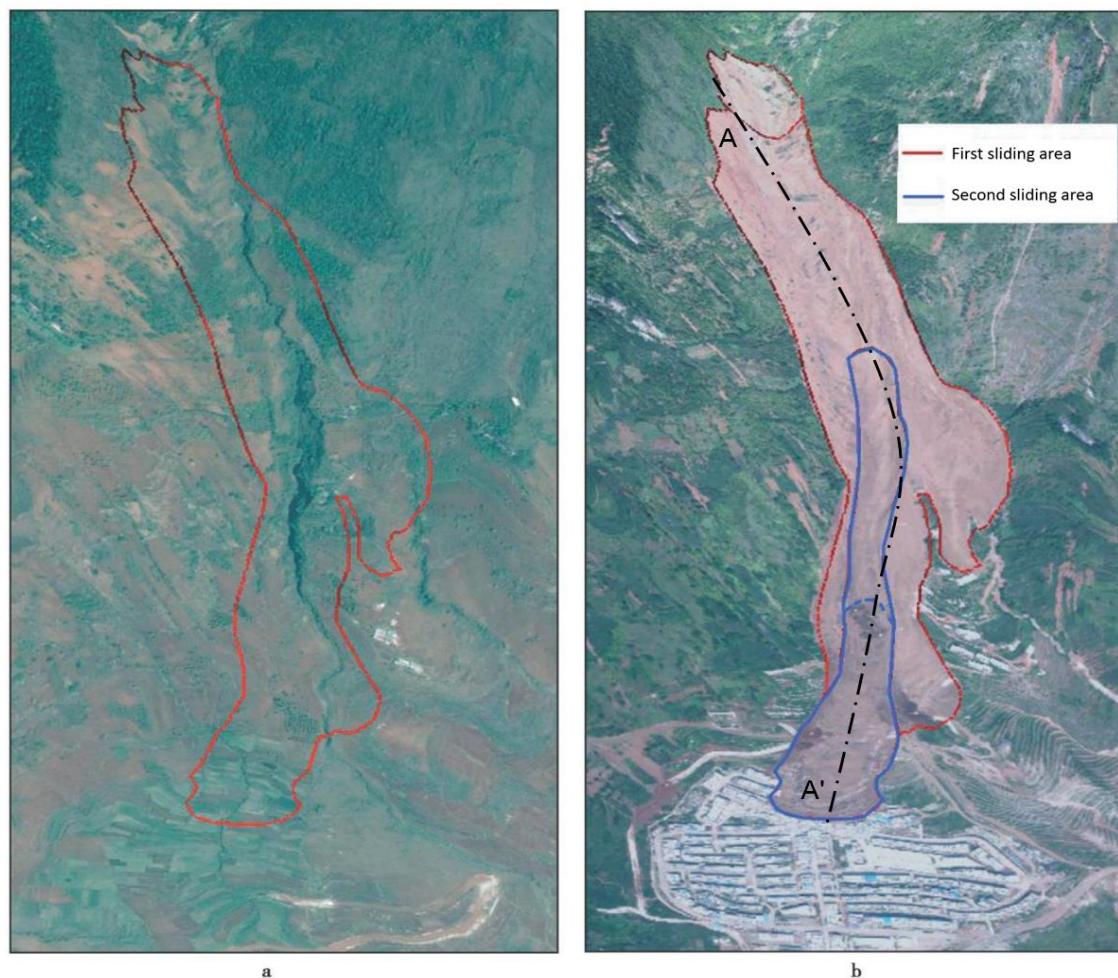


Figure 4. The remote sensing images before and after the Erman Mountain landslide[12].
a. before landslide; b. after landslide

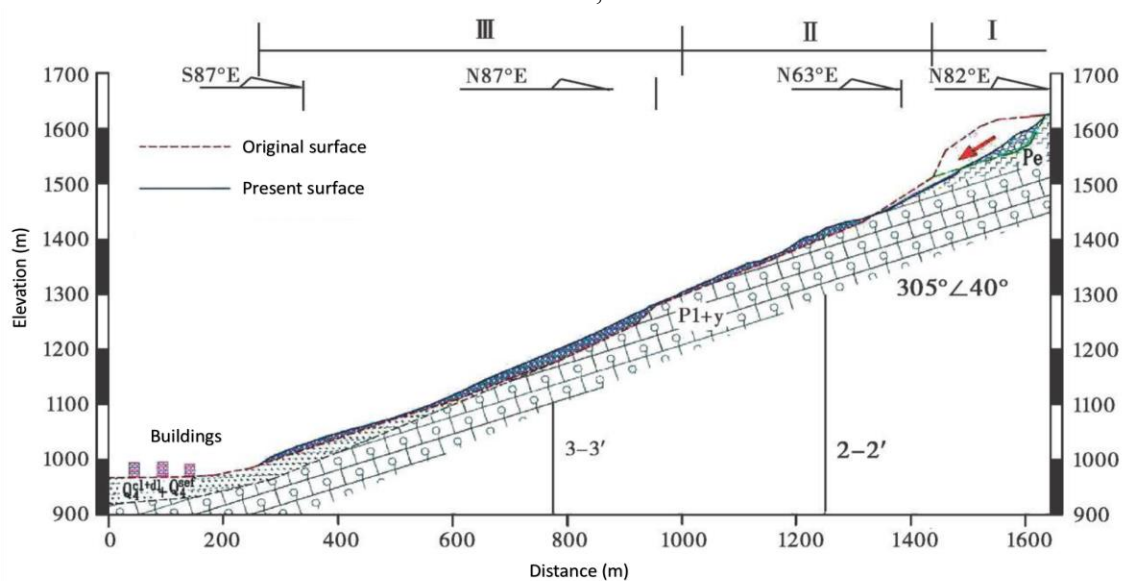


Figure 5. Longitudinal cross section (A-A') of Erman Mountain landslide [12].

In order to illustrate the capacity of the MPM in managing the long runout analysis, we simplified the profile of the section (A-A') to a constant slope model with the slope angle $\theta=25^\circ$, as shown in Figure 6. The model consists of two types of soil: the base soil and the weak soil. The material constants of the two types of soil are shown in Table 2. The weak soil is modelled with pure cohesive material to approximate undrained shearing behaviour.

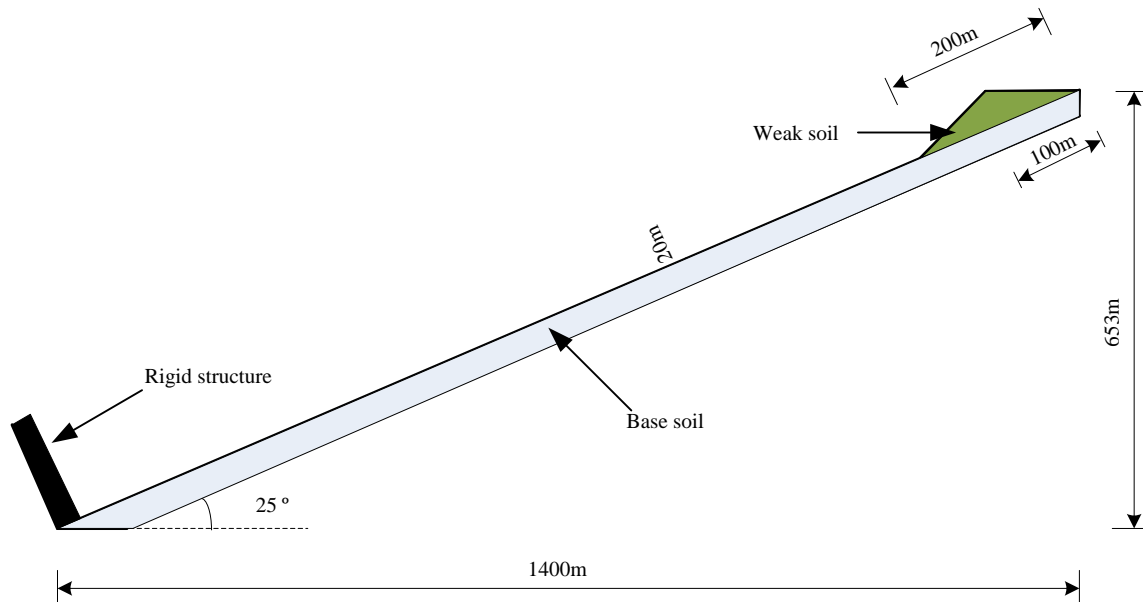


Figure 6. Simplified section (A-A') of Erman Mountain.

Table 2. Material constants of the soil

Soil type	ρ (kg/m ³)	E (MPa)	ν	c (kPa)	ϕ ($^\circ$)	ψ ($^\circ$)
Weak soil	2200	10	0.3	10	0	0
Base soil	2200	10	0.3	10	30	0

The numerical model is constructed in plane strain condition with fixed boundary conditions. The calculation is performed using square elements with the side length of $\Delta x=2\text{m}$ and a time step size of $\Delta t=2.557\times 10^{-4}\text{s}$. Initially, there are 4 material points per element. The initial stress field is generated using gravity loading by increasing the strength of the sliding soil.

Figure 7 shows the velocities of material points during the dynamic process of the landslide. The simulation of landslide take place at $t=0\text{s}$. Then the weak soil begins to slide down the slope with the velocity increasing rapidly. At $t=20\text{s}$ the front of the sliding soil impacts on the rigid structure with the maximum velocity of about 130 m/s. At this time, the kinetic energy reaches the maximum value of $1.7\times 10^7\text{kJ}$. From this time, the kinetic energy begins to decrease and the deposit becomes larger and larger. At $t=30\text{s}$ the deposit reaches the maximum height and the base soil far behind the front of the deposit is also sliding down with velocity decreasing with time. At about $t=50\text{s}$ the velocity of the soil is small and the deposit of the landslide reaches the maximum volume. The simulation lasted 75s and the final configuration of the computation is shown in Figure 8.

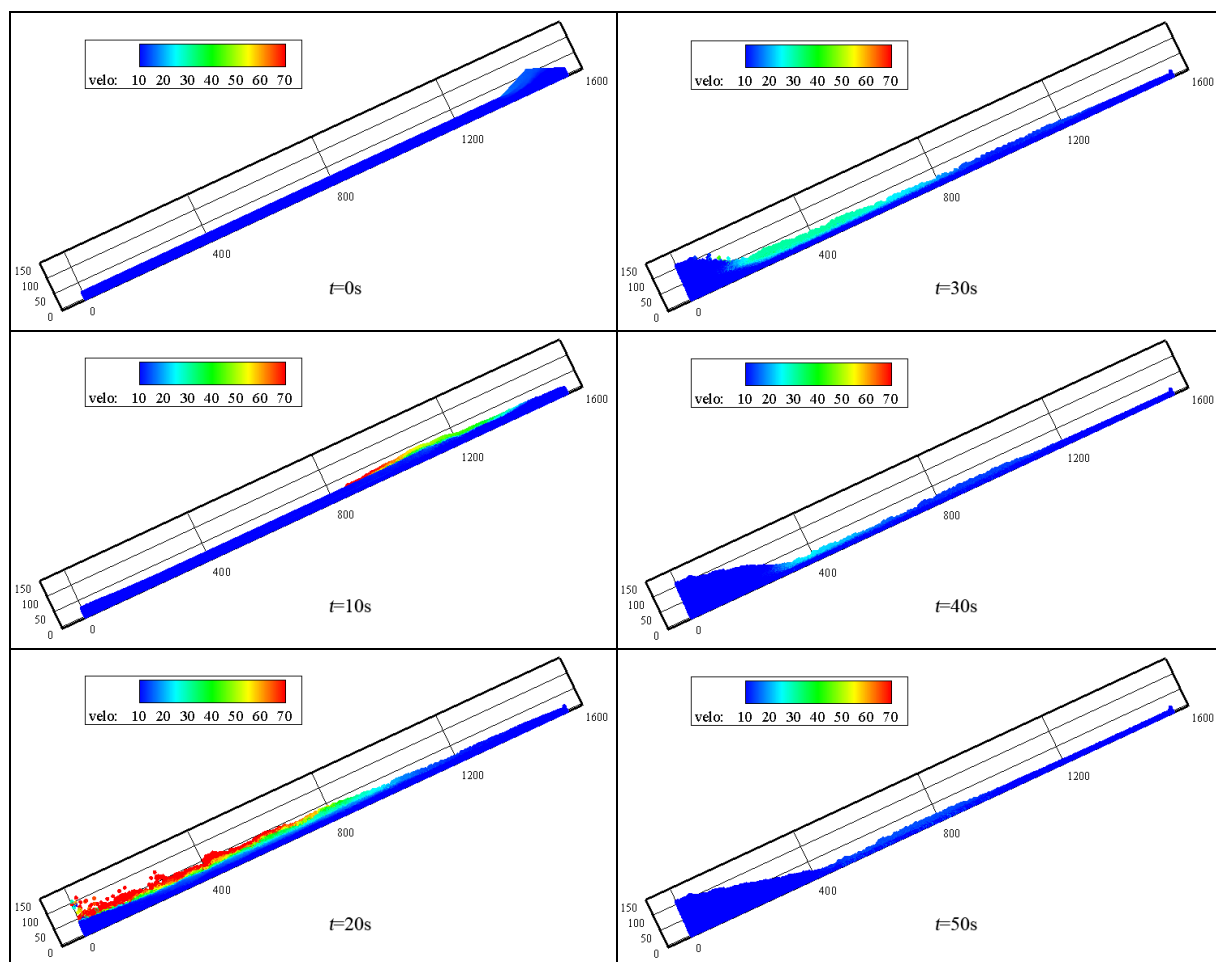


Figure 7. Velocity of sliding soil in Erman Mountain landslide (m/s)

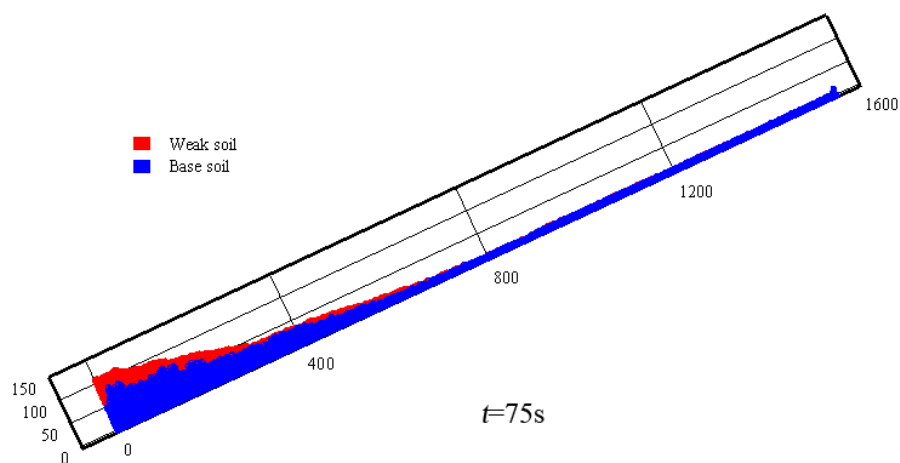


Figure 8. Final simulation configuration of Erman Mountain landslide

Figure 9 shows the impact force on the rigid structure. Before $t=20$ s, the impact force increases linearly with lower rate, because of the effect of the stress wave. From $t=20$ s to $t=30$ s the impact force

oscillates frequently due to the intense impact of the sliding soil. After $t=30$ s the impact force increases stably and reaches the peak value at $t=40$ s then decreases to the asymptotic value of 100MN/m.

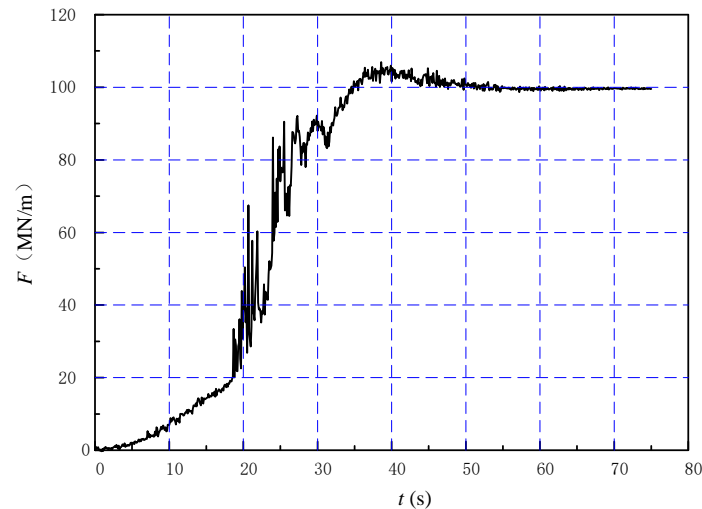


Figure 9. Impact force on the rigid structure of the landslide

4. Conclusions

Dynamic simulation of runout landslides by the MPM is presented. The MPM uses two representations of the continuum: Lagrangian representation of the material points and Eulerian description of the computational grid. Lagrangian scheme, which is convenient to record history-dependent variables in material constitutive model, is widely used in solid mechanics. Eulerian scheme, which avoids mesh distortion, is usually applied in fluid mechanics. The MPM combines the advantages of both Eulerian and Lagrangian descriptions and is very suitable for simulating long runout landslide.

Two numerical examples illustrate the capability of the MPM in runout analysis. It is inherent for MPM to model no-slip contact between different soil layers and contact. It is convenient to model the accumulation effect of the sliding soil and impact force on the structure. The velocities, affected areas, flow intensity are investigated.

Acknowledgements

This work was supported by the National Key Fundamental Research and Development Program of China (Project No. 2014CB047004).

References

- [1] Hungr O 1995 A model for the runout analysis of rapid flow slides, debris flows, and avalanches *Can. Geotech. J.* **32** 610-23
- [2] Coetzee CJ 2014 Discrete and continuum modelling of soil cutting *Comput. Part. Mech.* **1** 409-23
- [3] Mast CM, Arduino P, Miller GR and Mackenzie-Helnwein P 2014 Avalanche and landslide simulation using the material point method: flow dynamics and force interaction with structures *Comput. Geosci.* **18** 817-30
- [4] Sulsky D, Chen Z and Schreyer HL 1994 A particle method for history-dependent materials *Comput. Method. Appl. Mech. Eng.* **118** 179-196
- [5] Sulsky D, Zhou S and Schreyer HL 1995 Application of a particle-in-cell method to solid mechanics *Comput. Phys. Commun.* **87** 236-252
- [6] Harlow FH 1964 The particle-in-cell computing method for fluid dynamics *Methods Comput. Phys.* **3** 319-343

- [7] Andersen S, Andersen L 2010 Modelling of landslides with the material-point method *Comput. Geosci.* **14** 137-147
- [8] Bui HH, Fukagawa R, Sako K and Ohno S 2008 Lagrangian meshfree particles method (SPH) for large deformation and failure flows of geomaterial using elastic-plastic soil constitutive model *Int. J. Numer. Anal. Methods Geomech.* **32** 1537-1570
- [9] Liu P, Liu Y, Zhang X and Guan Y 2015 Investigation on high-velocity impact of micron particles using material point method *Int. J. Impact. Eng.* **75** 241-254
- [10] Belytschko T, Liu WK and Moran B 2000 Nonlinear finite elements for continua and structures *New York: John Wiley & Sons*
- [11] Coetzee CJ, Vermeer PA and Basson AH 2005 The modelling of anchors using the material point method *Int. J. Numer. Anal. Methods Geomech.* **29** 879-895
- [12] Xu Q Dong X Deng M Chen L and Hu Z 2010 The Ermanshan rock slide-debris flow of Junly 27, 2010 in Hanyuan, Sichuan: characteristics and failure mechanism *J. Eng. Geol.* **18** 609-622 (in Chinese)